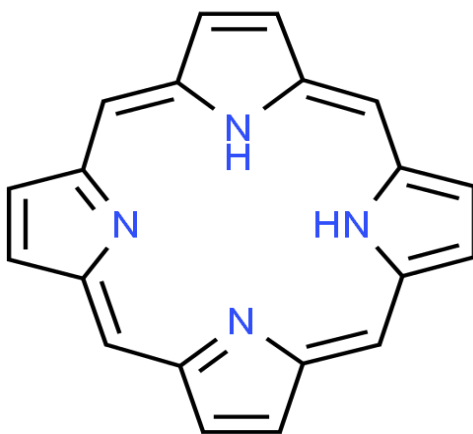University of Crete

Department of Materials Science and Technology

Bachelor Thesis:

"Porphyrin and aluminum porphyrin-based porous polymer networks for carbon dioxide capture and conversion"

Gaitanou Dimitra

Supervisor: Prof. Maria Vamvakaki

Heraklion, March 2020

Ευχαριστίες

Αρχικά θα ήθελα να ευχαριστήσω την επιβλέπουσα καθηγήτρια μου κ. Μαρία Βαμβακάκη για την ευκαιρία που μου έδωσε ώστε να βρίσκομαι στο εργαστήριο της και να πραγματοποιήσω εκεί την πτυχιακή μου εργασία. Επίσης θα ήθελα να ευχαριστήσω την κυρία Μαρία Καλύβα για την πολύτιμη βοήθεια της σε ότι και αν χρειάστηκα ακόμα και όταν εκείνη αγχωνόταν για μένα όταν εγώ δεν το έκανα. Με βοήθησε καθόλη τη διάρκεια της φοίτησης μου στο εργαστήριο σε πειραματικό και θεωρητικό επίπεδο και με βοήθησε να φέρω σε πέρας την πτυχιακή μου εργασία.

Έπειτα θα ήθελα να ευχαριστήσω τον κ. Γεράσιμο Αρματά για τη βοήθεια του στην ανάλυση και αξιολόγηση των πειραμάτων προσρόφησης καθώς και για τη συμμετοχή του στη διμελή μου επιτροπή.

Θα ήθελα να ευχαριστήσω όλο το group για το ευχάριστο κλίμα εντός εργαστηρίου τον Νίκο, τον Γιώργο, τον Γρηγόρη, τον Δημήτρη Γ., τη Μαρία Κ.. Ταυτόχρονα θα ήθελα να ευχαριστήσω τις φίλες και συνάδελφους που χωρίς την παρέα τους δεν θα περνούσε ευχάριστα η χρονιά την Μαρία Ψαρρού και την Εύα Βασιλάκη. Τέλος, θα ήθελα να ευχαριστήσω την καλή μου φίλη και συνάδελφο Μάγια Κοθρή, με την οποία είμασταν μαζί σε κάθε βήμα της δικής μου αλλά και της δικής της πτυχιακής. Περάσαμε τέλεια και ακόμα περνάμε!

Τέλος, θα ήθελα να ευχαριστήσω την οικογένεια μου για την υποστήριξη αλλά και την αγωνία που είχαν για εμένα, την αδερφή μου η οποία πιστεύει πιο πολύ απ' όλους σε εμένα αλλά και τους φίλους μου εκτός εργαστηρίου που με στήριξαν ώστε να τελειώσω την πτυχιακή μου εργασία αλλά και κατά τη διάρκεια των σπουδών μου.

Table of Contents

Abstract

During the past decades, environmental issues have attracted a lot of research and technological interest due to the climate changes, global warming and limitations of the energy resources. The rising levels of CO_2 emissions which cause global warming, demand the development of novel processes based on advanced materials for CO_2 capture and conversion. Porous organic polymers with appropriate properties, including large surface areas, narrow pore size distribution, high chemical and thermal stability and functional groups are excellent candidates for potential applications in CO_2 capture and conversion. In this work, we present the synthesis of porous polymer networks based on porphyrin (Po) and aluminum porphyrin (Al-Po) moieties. The development of the porous polymeric materials is based on the synthesis of a tetra-methacrylate porphyrin cross-linker. The porous porphyrin network (Po-net) was synthesized by free-radical polymerization of the tetra-methacrylate porphyrin derivative using azobisisobutyronitrile (AIBN) as the initiator. Next, the aluminum porphyrin-based network (Al-Po-net) was synthesized by the metalation of the Po-net using dimethylaluminum chloride. After drying the networks under supercritical CO_2 conditions, the morphology of the Po and Al-Po-net was characterized by scanning electron microscopy (SEM), while the successful network metalation was verified by Attenuated Total Reflection Fourier-transform infrared (ATR-FTIR) spectroscopy and by Energy-dispersive X-ray spectroscopy (EDS). The porous Po-net showed a high BET surface area of 622 m^2g^{-1}, while that of the Al-Po-net was lower at 167 m^2g^{-1}. Furthermore, the porous Po-net showed higher CO_2 absorption in comparison with the Al-Po-net, 1.54 mmol/g and 0.64 mmol/g, respectively at 273 K. The catalytic performance of both polymeric networks, Po and Al-Po, was investigated for the cycloaddition of CO_2 in epichlorohydrin using tetrabutylammonium bromide as a co-catalyst. The conversion of epichlorohydrin to the carbonate derivative was determined by proton nuclear magnetic resonance (^{1}H -NMR) spectroscopy. The experimental results showed a high catalytic activity of Al-Po-net with a 93% conversion at 100ºC, 1 atm and 24 h reaction time, while the Po-net exhibited a similar good performance with 88% conversion under the same reaction conditions.

The catalytic conversion of epichlorohydrin to the cyclic carbonate was found to increase with the reaction temperature.

1. Introduction

1.2 Porous materials

Porous materials have drawn a lot of attention over the last decades for their wide potential applications in catalysis[1], gas capture, separation and storage[2],[3]. Due to the presence of pores and their high surface area, porous materials exhibit very different properties compared to their bulk counterparts such as novel optical, chemical and electronic behavior. Based on their pore size, porous materials can be divided into the following three categories: microporous with pore diameter Dp < 2 nm , mesoporous with 2 nm < Dp < 50 nm and microporous with Dp > 50 nm[4],[5]. Porous materials can also be categorized according to their framework into inorganic, organic and hybrid (organic-inorganic) materials.

The most important microporous inorganic crystalline materials are the zeolites. Zeolites have large surface areas, high ion exchange capacity and narrow pore-size distributions which render then very attractive heterogeneous catalysts and excellent materials for gas sorption.[6],[7]

Metal-organic frameworks (MOFs) are organic-inorganic (hybrid) porous materials that have attracted a lot of attention in the field of material science due to their distinct structure. MOFs can be synthesized by various methods such as solvothermal, ultrasonic, microwave treatment, etc. under mild conditions. Because of their structure MOFs present unique properties such as high porosity, accessible pores, stability against air, etc. MOFs are often used in gas storage and separation, heterogeneous catalysis and photocatalysis, etc.[8]

1.2 Porous organic polymers

Porous organic polymers (POPs) are porous materials synthesized from organic monomers and have become very popular over the last years due to their porous nature, great physicochemical stability, chemical functionality and high diversity in structure. POPs can be divided into five

groups, hypercrosslinked polymers (HPCs), conjugated microporous polymers (CMPs), covalent organic frameworks (COFs), triazine-based frameworks and polymers of intrinsic microporosity (PIMs).[9] There are many methods to synthesize porous polymers via solvothermal treatment, free radical polymerization[10], emulsion polymerization[11], suspension polymerization[12] or high internal phase emulsion.[13]

The most common application of POPs is in gas separation such as CO_2/N_2 and CH_4/CO_2 separation. Gas separation occurs due to the different interactions between the porous materials and the gas molecules or the fact that different sizes of the molecules can be eliminated from the pores of the material or an assemblage of the above. Moreover, POPs are used as catalysts due to their designability and functionalization.[14]

1.3 Porphyrins and metalloporphyrins

Porphyrins have drawn a lot of attention over the last years, because they are omnipresent in natural systems and have great potential for use in different applications such as catalytic reactions, solar energy conversion, etc. The word porphyrin originates from the Greek word porphyra which means purple. As the name signifies porphyrins have a deep purple color and they can either be found in Nature or can be synthesized. They comprise four pyrrole rings linked by four methine bridges and an aromatic macrocycle ring.[15] **(Scheme 1.1)**
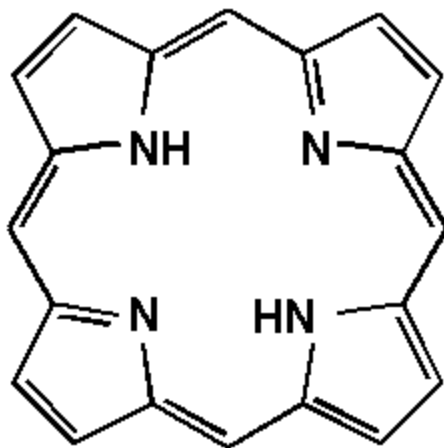
Scheme 1.1 Structure of porphyrin

Metalloporphyrins have also attracted a lot of attention lately due to their interesting catalytic performance in chemistry and biology.[16] By adding a metal into the porphyrin framework new properties are attained expanding their use in other fields, such as the use of Mn- and Gd-porphyrins in MRI, etc.[17] Some of the applications that porphyrins and metalloporphyrins share is their use in electron transfer, catalysis, gas separation and storage, optoelectronic devices, etc.[15]

1.4 Porous porphyrin-based networks

Porphyrin-based nanoporous polymer networks have been synthesized resulting in BET surface areas of 910 m^2/gr.[18] Polyporphyrins have been also synthesized reaching surface areas as high as 1522 m^2/g and hydrogen uptake measurements revealed a slight increase in the heat of adsorption after the insertion of Fe(II) ions into the porphyrin rings.[19] In another study, porphyrin-based hyperbranched polyimides were synthesized via a Sander Maier reaction and exhibited BET surface areas up to 682 m^2/gr[20]

1.5 Carbon dioxide (CO_2) capture and conversion

 During the last years, large amounts of CO_2 have been released into the atmosphere due to human interventions such as combustion of transportation of fuels. These high levels of CO_2 have several consequences such as the climate change, including lowering the pH of the oceans. In order to decrease the pollution, technology has found ways to capture CO_2 and convert it into other more valuable chemicals.[21] Furthermore, CO_2 is an important feedstock in the synthetic process of cyclic carbonate from epoxy compounds using different catalysts. Since cyclic carbonate compounds can be applied in various industrial areas including aprotic solvents, precursors for polycarbonate synthesis, and intermediates in organic synthesis, the development of effective catalysts for the conversion of epoxy compounds to cyclic carbonates is of great importance for practical applications.[22]

1.6 Catalysis

According to IUPAC, a catalyst is a substance that increases the reaction rate without altering the total standard Gibbs energy.[23] In most cases, the catalyst creates a different, faster path for the reaction. Because the catalyst is not consumed in the process, each molecule can participate in many consecutive cycles, so only a small amount of catalyst is needed relative to the substrate. The substrate / catalyst ratio reflects the efficiency of the catalyst, which is measured as Turnover Number: TON, or Turnover Frequency (TOF) if the time factor is taken into account. There are many different types of catalysts, such as proton (H^+) and Lewis acids or even organometallic complexes, organic or inorganic polymers and enzymes. To simplify things, catalysis has been divided into three categories: homogeneous catalysis, heterogeneous catalysis and biocatalysis. Although the catalysts and process conditions in each category may be very different, the principles of each type of catalyst are the same. The main advantages of catalysis are that the desired product is consumed faster, using fewer resources and producing less waste because in most cases the catalyst opens a selective path to the desired product. There are different types of product selectivity. Chemoselectivity indicates a situation where two different chemical reactions can occur, yielding two different products. Site selectivity occurs when the same chemical reaction in different regions of the molecule results in different products. When a reaction yields two (or more) diastereomers, the selectivity in each of them is called diastereoselectivity, whereas in the specific case where the two products are enantiomers, we are talking about enantioselectivity. Catalysts can exist in different states, depending on their degree of oxidation, water content etc. These states have different physicochemical properties and different capacities to accelerate reactions. Industrial chemical reactions take place in the presence of solid catalysts, which can dramatically accelerate these reactions.

1.7 CO_2 cycloaddition reaction

The CO_2 cycloaddition reaction requires an acid catalyst (either Lewis or Brønsted acid). The use of homogeneous catalysts is a major problem in the industry as their separation from the reaction solution is arduous and costly. It is quickly understood that the existence of suitable heterogeneous catalysts with Lewis or Brønsted acidity is necessary.
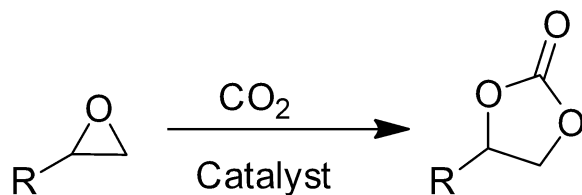
Scheme 1.2 Cycloaddition reaction of CO_2 to epoxides to form cyclic carbonates.

1.8 Mechanism of cycloaddition reaction of CO_2 to epoxides

The catalytic synthesis of cyclic carbonates from CO_2 takes place in four steps which are analyzed below giving the whole mechanism schematically in **Scheme 1.6**. The four steps are the following:

1. First, the dual activation of the epoxide takes place fast, by the coordinative interaction between the oxygen atom of the epoxide and the Lewis acid aluminum site of the catalyst.

2. At the same time, the nucleophile (Br⁻) from TBAB attacks the less-hindered side of the epoxide in order to open the epoxy ring, producing an intermediate Al-coordinated bromo alkoxide. (Scheme 1.3)
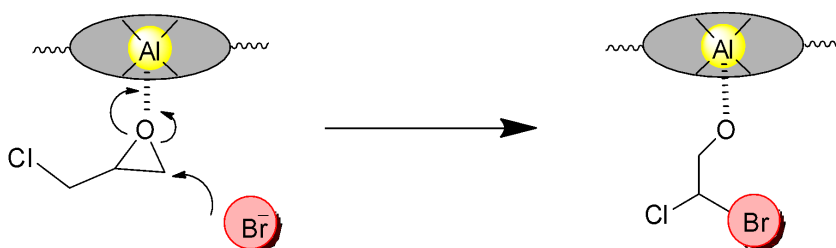
Scheme 1.3

3. Next, the intercalation of the CO_2 in the porous network into the above intermediate causes the formation of a metal carbonate specie. (Scheme 1.4)
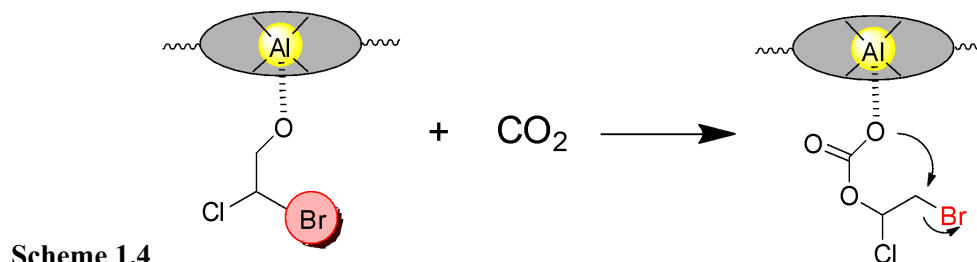
Scheme 1.4

4. Finally, the catalytic cycle is completed by an intramolecular S_N2 cyclization, producing the carbonate and simultaneously releasing the Br⁻ while the Al-Po-net is recovered. (Scheme 1.5)
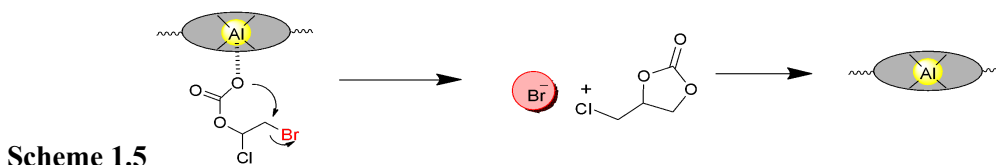
Scheme 1.5

The above steps are summarized in the Scheme below. (Scheme 1.6)[2]
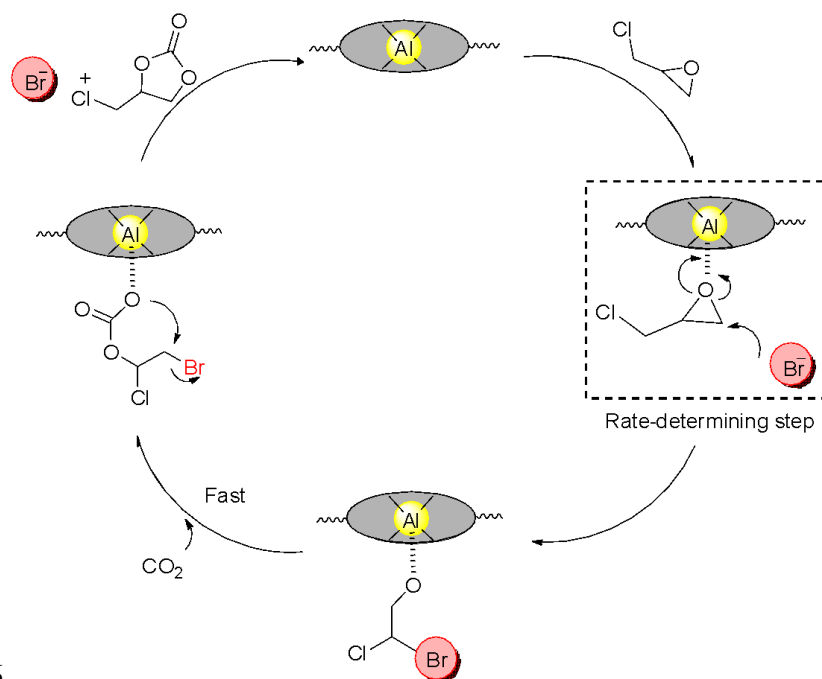
Scheme 1.6

Also, below is the way how TBAB catalyzes the conversion of an epoxide to a cyclic carbonate using CO_2 (Scheme 1.7) [24]:
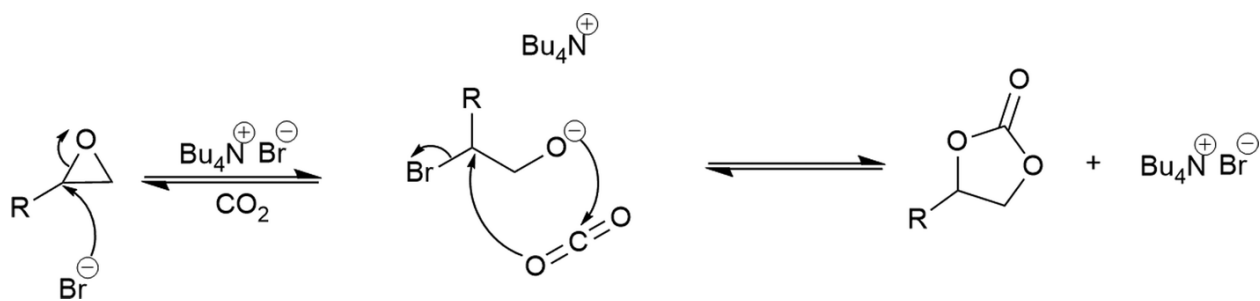
Scheme 1.7 Conversion of an epoxide to a cyclic carbonate catalyzed by TBAB.

1.9 Current study

Lately, the interest in porous materials for gas purification, gas capture and conversion has highly increased. In response to this, the present work provides a simple and facile process to produce highly cross-linked networks that exhibit a sufficient internal surface area and are potential candidates for use in the capture and conversion of carbon dioxide. This work focuses on the synthesis of highly cross-linked porphyrin networks by a typical free-radical polymerization process. In order to prepare the polymer networks a tetra-methacrylate porphyrin derivative was prepared by the reaction of 5, 10, 15, 20-tetrakis (4-hydroxyphenyl)-21H, 23H-porphine with methacryloyl chloride. The successful preparation of the tetra-methacrylate porphyrin cross-linker was confirmed by ^{1}H NMR spectroscopy. The functionalized porphyrin was further polymerized by free radical polymerization using AIBN as the initiator resulting in porous porphyrin networks (Po-net). Afterwards, a typical metalation process took place for the introduction of aluminum ions (Al^{+3}) into the porphyrin ring, producing aluminum porphyrin networks (Al-Po-net). In order to obtain solvent-free open pore samples a supercritical point drying process was employed. The morphology of the porphyrin and aluminum porphyrin network was examined by scanning electron microscopy (SEM). The internal surface area of the porous network was investigated using N_2 adsorption-desorption measurements, while the CO_2 adsorption capacity of both Po-net and Al-Po-net was examined. Finally, the catalytic performance of both Po-net and Al-Po-net was investigated in a cycloaddition reaction of CO_2 to epichlorohydrin.

1.10 References

1.   Kaur P, Hupp JT, Nguyen ST. Porous Organic Polymers in Catalysis: Opportunities and Challenges. *ACS Catal*. 2011;1(7):819-835. doi:10.1021/cs200131g

2.   Zhang K, Tieke B, Vilela F, Skabara PJ. Conjugated Microporous Networks on the Basis of 2,3,5,6-Tetraarylated Diketopyrrolo[3,4-c]pyrrole. *Macromol Rapid Commun*. 2011;32(11):825-830. doi:10.1002/marc.201100045

3.   Dawson R, Cooper AI, Adams DJ. Chemical functionalization strategies for carbon dioxide capture in microporous organic polymers: CO_2 capture in microporous organic polymers. *Polym Int*. 2013;62(3):345-352. doi:10.1002/pi.4407

4.   Polarz S, Antonietti M. Porous materials via nanocasting procedures: innovative materials and learning about soft-matter organization. *Chem Commun*. 2002;(22):2593-2604. doi:10.1039/b205708p

5.   Fan X, Jiao Y. Porous Materials for Catalysis. In: *Sustainable Nanoscale Engineering*. Elsevier; 2020:115-137. doi:10.1016/B978-0-12-814681-1.00005-9

6.   Carreon MA, Li S, Falconer JL, Noble RD. Alumina-Supported SAPO-34 Membranes for CO $_2$ /CH $_4$ Separation. *J Am Chem Soc*. 2008;130(16):5412-5413. doi:10.1021/ja801294f

7.   Salleh WNW, Ismail AF, Matsuura T, Abdullah MS. Precursor Selection and Process Conditions in the Preparation of Carbon Membrane for Gas Separation: A Review. *Sep Purif Rev*. 2011;40(4):261-311. doi:10.1080/15422119.2011.555648

8.   Ali Akbar Razavi S, Morsali A. Linker functionalized metal-organic frameworks. *Coord Chem Rev*. 2019;399:213023. doi:10.1016/j.ccr.2019.213023

9.   Li G, Meng X, Wang J, et al. A low-cost and high-efficiency carbazole-based porous organic polymer as a novel sorbent for solid-phase extraction of triazine herbicides in vegetables. *Food Chem*. 2020;309:125618. doi:10.1016/j.foodchem.2019.125618

10.   Lei Y, Zhang M, Leng G, Ding C, Ni Y. SO3H-functionalized porous organic polymer with amphiphilic and swelling properties: A highly efficient solid acid catalyst for organic transformations in water. *Microporous Mesoporous Mater*. 2020;299:110110. doi:10.1016/j.micromeso.2020.110110

11.   Sun J-K, Antonietti M, Yuan J. Nanoporous ionic organic networks: from synthesis to materials applications. *Chem Soc Rev*. 2016;45(23):6627-6656. doi:10.1039/C6CS00597G

12.   Lee C, Nam E, Chae H. Photo-stable cross-linked micron bead with functionalized quantum via suspension polymerization for color conversion. *Polymer*. 2019;177:19-24. doi:10.1016/j.polymer.2019.05.059

13.   Wang C, Pei X, Tan J, et al. Thermoresponsive starch-based particle-stabilized Pickering high internal phase emulsions as nutraceutical containers for controlled release. *Int J Biol Macromol*. 2020;146:171-178. doi:10.1016/j.ijbiomac.2019.12.269

14.   Li M, Zhao H, Lu Z-Y. Porphyrin-based porous organic polymer, Py-POP, as a multifunctional platform for efficient selective adsorption and photocatalytic degradation of cationic dyes. *Microporous Mesoporous Mater*. 2020;292:109774. doi:10.1016/j.micromeso.2019.109774

15.   Giovannetti R. The Use of Spectrophotometry UV-Vis for the Study of Porphyrins. In: Uddin J, ed. *Macro To Nano Spectroscopy*. InTech; 2012. doi:10.5772/38797

16.   Sehgal P, Narula AK. Metal substituted metalloporphyrins as efficient photosensitizers for enhanced solar energy conversion. *J Photochem Photobiol Chem*. 2019;375:91-99. doi:10.1016/j.jphotochem.2019.02.003

17.   Shao S, Rajendiran V, Lovell JF. Metalloporphyrin nanoparticles: Coordinating diverse theranostic functions. *Coord Chem Rev*. 2019;379:99-120. doi:10.1016/j.ccr.2017.09.002

18.	McKeown NB, Hanif S, Msayib K, Tattershall CE, Budd PM. Porphyrin-based nanoporous network polymers. *Chem Commun*. 2002;(23):2782-2783. doi:10.1039/b208702m

19.	Xia J, Yuan S, Wang Z, et al. Nanoporous Polyporphyrin as Adsorbent for Hydrogen Storage. *Macromolecules*. 2010;43(7):3325-3330. doi:10.1021/ma100026f

20.	Shi K, Song N, Zou Y, et al. Porphyrin-based porous polyimides: Synthesis, porous structure, carbon dioxide adsorption. *Polymer*. 2019;169:160-166. doi:10.1016/j.polymer.2019.02.062

21.	Grice KA. Carbon dioxide reduction with homogenous early transition metal complexes: Opportunities and challenges for developing CO 2 catalysis. *Coord Chem Rev*. 2017;336:78-95. doi:10.1016/j.ccr.2017.01.007

22.	Qu R, Ren Z, Li N, Zhang F, Zhang ZJ, Zhang H. Solvent-Free cycloaddition of carbon dioxide and epichlorohydrin catalyzed by surface-attached imidazolium-type poly(ionic liquid) monolayers. *J CO2 Util*. 2020;38:168-176. doi:10.1016/j.jcou.2020.01.022

23.	Laidler KJ. A glossary of terms used in chemical kinetics, including reaction dynamics (IUPAC Recommendations 1996). *Pure Appl Chem*. 1996;68(1):149-192. doi:10.1351/pac199668010149

24.	Supasitmongkol S, Styring P. A single centre aluminium(III) catalyst and TBAB as an ionic organo-catalyst for the homogeneous catalytic synthesis of styrene carbonate. *Catal Sci Technol*. 2014;4(6):1622-1630. doi:10.1039/C3CY01015E

2. Experimental

2.1 Materials

5, 10, 15, 20-Tetrakis (4-hydroxyphenyl)-21H, 23H-porphine (PO-(OH)$_4$, 95%), methacryloyl chloride (MCl, 97%, Fluka) and ethanol (absolute, 98%) were obtained from Sigma-Aldrich and N, N-Dimethylformamide (extra pure, 99.9%), triethylamine (synthesis grade, 99%), and tetrahydrofuran were purchased from Scharlau. 2,2′-Azobis(2-methylpropionitrile) (98%) was used as the initiator and was purchased by Acros Organics. Diethylaluminium chloride, 0.9 M solution in toluene was purchased by Acros Organics. (±)- Epichlorohydrin purum (≥99%) was used as the substrate in catalysis and was purchased by Sigma-Aldrich. Tetrabutylammonium bromide (TBAB) was used as a co-catalyst and was purchased from Sigma-Aldrich. The Tables below depict the chemical structures of the main chemicals used for the porphyrin functionalization and the cross-linkers and initiator used for the porous porphyrin networks synthesis.

Table 2.1. Chemical structures of the chemicals used for the synthesis of the tetra-methacrylate porphyrin derivative.
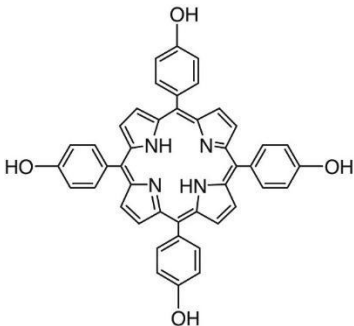
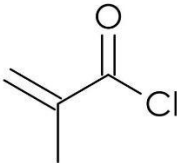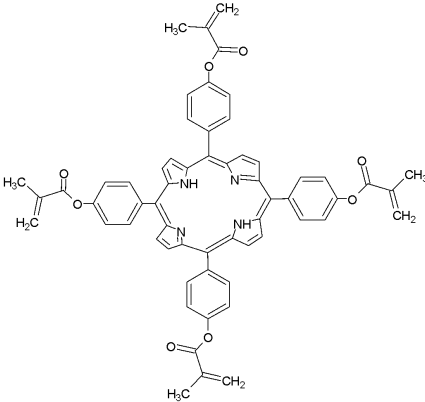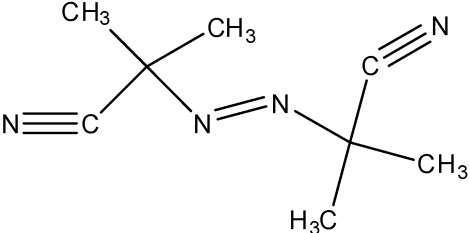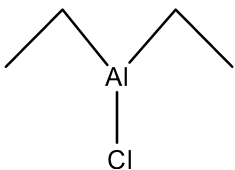| 5, 10, 15, 20-Tetrakis (4-hydroxyphenyl)-21H, 23H-porphine | Methacryloyl chloride |

Table 2.2 Chemical structures of the tetra-methacrylate porphyrin derivative and the initiator used for the synthesis of the porous Po-net and of the aluminum salt used for the synthesis of Al-Po-net.

tetra-methacrylate porphyrin derivative	2,2′-Azobis(2-methylpropionitrile)
Diethylaluminium chloride	

2.2 Synthesis of the tetra-methacrylate porphyrin derivative

The tetra-methacrylate porphyrin derivative that acted as a cross-linker for the synthesis of the Po-nets was synthesized by the esterification reaction of PO-(OH)$_4$, with MCl. In a typical procedure, PO-(OH)$_4$ (1.0408 g, 0.0015 mol), dried overnight under vacuum in a 100 ml round-bottom flask, was dissolved in 70 ml dry THF. The above solution was stirred until complete dissolution of the PO-(OH)$_4$, followed by the addition of 17 ml (12.336 g, 0.12 mol) TEA. Next, MCl (1.5 ml, 0.015mol) was added to the above mixture at 0 ºC under stirring. The reaction was allowed to proceed overnight at room temperature under continuous stirring. The next day, the reaction mixture was filtered under nitrogen to remove the triethylamine hydrochloride salt formed, while the excess TEA and THF were removed under reduced pressure.

The final product was dried under vacuum (0.5686 g, yield ~40%) and was characterized by ^{1}H NMR spectroscopy. ^{1}H NMR (300MHz, CDCl$_3$, δ) 2.82 (s, 2H), 2.23 (s, 12H), 5.91 (s, 4H), 6.56 (s, 4H), 7.54 (d, 8H), 8.22 (d, 8H), 8.90 (s, 8H).

2.3 Synthesis of porphyrin-based networks

The Po-net was prepared by free radical polymerization. First, the tetra-methacrylated porphyrin derivative (0.5686 g, 0.594 mmol) was added in a 22 ml vial. Next, 15 ml DMF were added followed by the addition of AIBN (0.0039 gr, 0.0000238 mol). Finally, the reaction mixture was degassed for 20 min and the reaction was allowed to take place for 2 days at 60 ^{o}C. The porphyrin network was washed with DMF to remove any unreacted crosslinker.

2.4 Synthesis of aluminum porphyrin-based networks

The metalation of the porphyrin network took place in a 100ml round bottom flask which was burnt with a blowtorch under vacuum to remove possible humidity. After that, the Po-net (0.1854 gr, 0.00019 mol) was added in the flask and was purged with N$_2$ for 30 min. Next, 6 ml dry DMF were added under constant stirring and under a N$_2$ atmosphere followed by the addition of diethylaluminum chloride (Et$_2$AlCl 0.9 M solution in toluene, 0.25 ml, 0.000225 mol). The reaction was allowed to proceed overnight at room temperature under continuous stirring. The aluminum porphyrin network, Al-Po-net, was next purified by washing with DMF and was recovered by centrifugation.

2.5 Preparation of porous Po-net and Al-Po-net by supercritical point drying (SPD)

A Bal-Tec CPD 030 critical point dryer was used for carrying out the drying process. The drying procedure involved first the exchange of ethanol (where Po-net and Al-Po-net were dispersed) with liquid CO$_2$ using a plastic tube with 2 filters on each side, at 8 ^{o}C over an extended period of time (8 h). Finally, CO$_2$ was removed under supercritical conditions to obtain the open pore Po-net and Al-Po-net networks, by leaving the sample for 2.5 h at 41 ^{o}C and 91.3 bar (supercritical conditions) and by gassing out for a period of 55 min.

2.6 Catalytic performance

A typical catalytic reaction was employed according to the following process. First, a vial filled with epichlorohydrin was purged with CO$_2$ for 30 min. Meanwhile, the catalyst, Po-net or

Al-Po-net, and TBAB as the co-catalyst were added into a 22 ml vial which was purged with CO_2 for 20 min. Finally, epichlorohydrin (0.25 ml, 3.2 mmol) was added into a vial contained 0.25 mol% catalyst and 2 mol% co-catalyst. The catalytic reaction was allowed to take place for 24 h at 100 °C. The conversion of epichlorohydrin to the carbonate was determined by ^{1}H NMR spectroscopy.

2.7 Sample Characterization

2.7.1 Scanning Electron Microscopy (SEM)

Scanning electron micrographs were recorded using a field-emission JEOL 7000 electron microscope operating at 10 kV. Samples were prepared by diluting the gel dispersion in ethanol and depositing a drop of the dispersion onto a silicon wafer and allowing it to dry in air overnight. The slides were then sputter-coated with a 10 nm Au film to reduce charging during the measurements.

2.7.2 Attenuated total reflection Fourier transform infrared (ATR-FTIR) spectroscopy

FT-IR spectroscopy is used to identify the chemical composition of a material or whether a reaction is complete. In this study, FTIR spectroscopy was used in order to identify the chemical structure of the Po-net and Al-Po-net networks and also whether the aluminum ion was introduced within the porphyrin macrocycle. The measurements were performed in the frequency range between 550 and 4000 cm^{-1} and 128 scans were collected for each spectrum. A background scan of 32 scans was recorded prior to each measurement and was subtracted from the sample spectra.

2.7.3 Nuclear Magnetic Resonance (NMR) spectroscopy

A 500 MHz Bruker ^{1}H NMR spectrometer was used for the measurements. The samples were dissolved in deuterated chloroform (chloroform-d) and were then transferred into an NMR tube in order to perform the measurements.

2.7.4 Gas adsorption isotherms

Gas adsorption experiments were conducted using a Quantachrome Model NOVA 3200e Gas Sorption Analyzer. Nitrogen and carbon dioxide gases were selected as the adsorbates. The gas adsorption data were analyzed using the multipoint BET gas adsorption theory in order to determine the surface area of the samples. The non-local Density Functional Theory (NLDFT) method was employed to determine the pore volume of the samples. Before the measurement the samples were outgassed at 80 $^{\circ}$C under vacuum for 12 h. The N_2 isotherms were obtained using a liquid nitrogen bath (at 77 K) while, the CO_2 adsorption measurements took place at 273 K.

2.7.5 Diffuse reflectance UV/Vis spectroscopy

The optoelectronic properties of the solid networks were studied by diffuse reflectance UV/Vis spectroscopy. The instrumentation used is a Shimadzu UV-2401 PC UV/Vis Spectrometer. The material used as reference is $BaSO_4$ and measurements were conducted by coating the powder sample on top of the $BaSO_4$ base material. The reflectance of the samples was measured in the range of 300 to 800 nm.

3. Results and Discussion

3.1 Synthesis of the tetra-methacrylated porphyrin derivative

An esterification reaction was carried out for the functionalization of the porphyrin molecule to a tetra-methacrylate analogue, using methacryloyl chloride. Triethylamine was used to bind the HCl formed during the esterification reaction and precipitated as a salt in the organic reaction medium thus pushing the reaction to quantitative yield (Scheme 3.1)
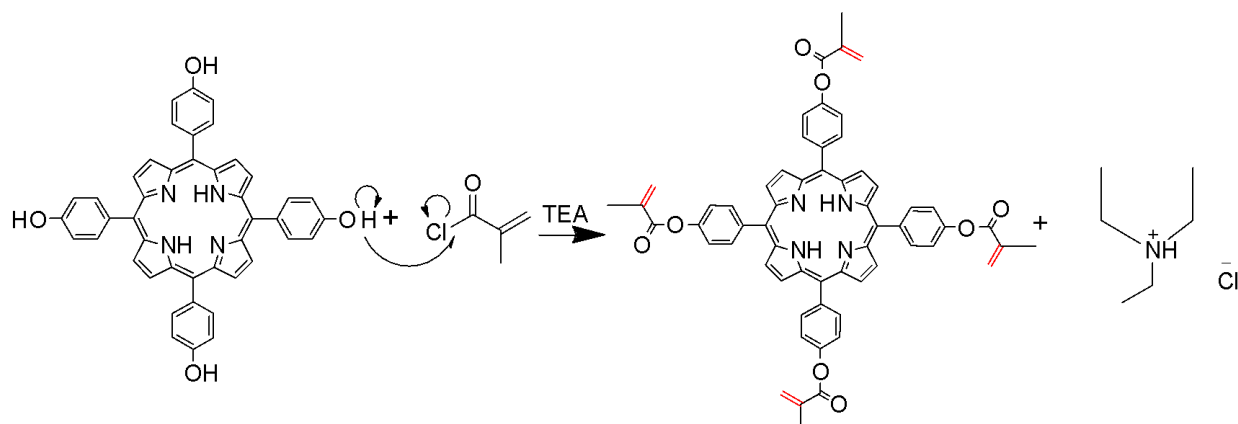
Scheme 3.1 Schematic representation of the synthesis of the tetra-methacrylate porphyrin derivative.

The successful synthesis of the tetra-methacrylate porphyrin derivative was confirmed by ^{1}H NMR spectroscopy (Figure 3.1). The peak at 8.93 ppm corresponds to the 8 protons of the porphyrin macrocycle and the peaks at 7.57 and 8.25 ppm are assigned to the protons of the four phenyl groups of the porphyrin. The peak at 2.23 ppm corresponds to the twelve protons of the methyl groups of the incorporated methacrylate moieties, whereas the peaks at 5.93 and 6.58 ppm correspond to the protons of the methylene group of the methacrylate groups. The above assigned peaks and the lack of any additional peaks verify the successful synthesis of the functional polymerizable porphyrin molecules.
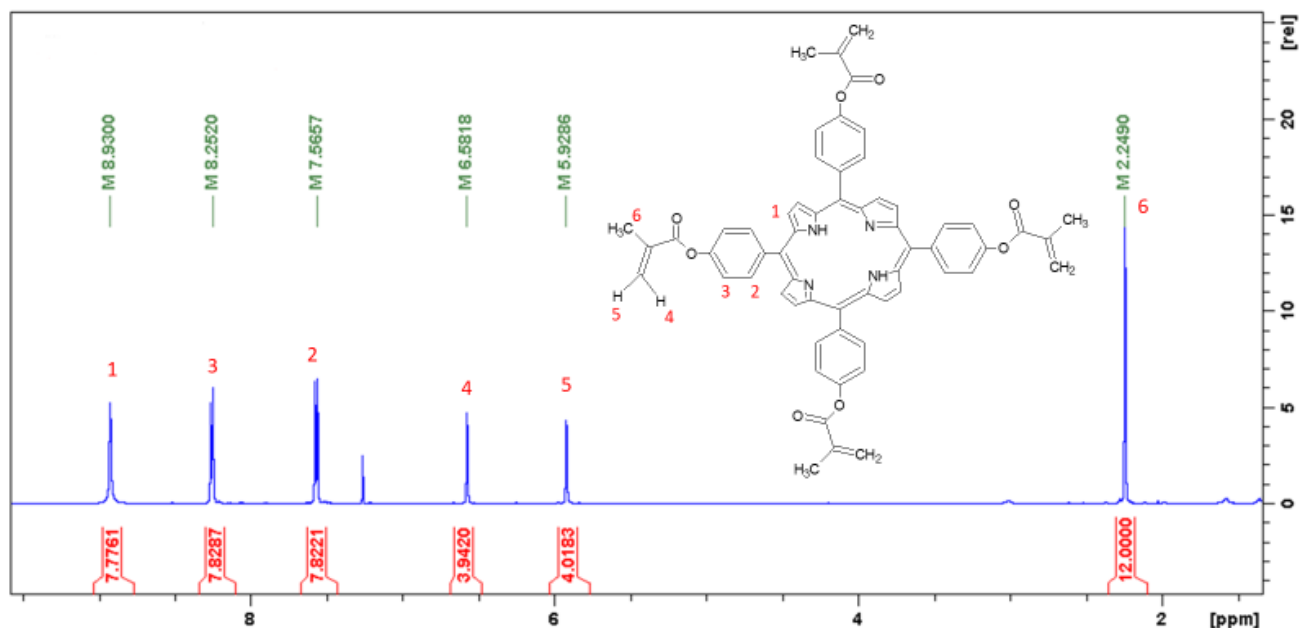
Figure 3.1 ^{1}H NMR spectrum of the tetra-methacrylated porphyrin derivative in CDCl$_3$.

3.2 Synthesis of the porphyrin network

In order to synthesize the porphyrin network, a free radical polymerization was used in which the tetra-methacrylate porphyrin served as the monomer/cross-linker and AIBN as the initiator. The polymerization took place at 60 °C for 2 days.

3.3 Synthesis of the aluminum porphyrin network

The metalation of the porphyrin network took place by the reaction the Po-net with diethylaluminum chloride. The reaction was allowed to proceed overnight at room temperature under continuous stirring. The obtained Al-Po-net network was purified by washing with DMF and was recovered by centrifugation.

3.4 Supercritical point drying of Po-net and Al-Po-net

After synthesis, the solvent-free open pores of the networks were obtained by supercritical point drying with CO$_2$. The drying procedure involved first the exchange of the solvent from ethanol (in which Po-net and Al-Po-net were dispersed) with liquid CO$_2$ at 8 °C over an extended period of time (8 h). Finally, CO$_2$ was removed under supercritical conditions to obtain the open pore

Po-net and Al-Po-net networks by leaving the samples for 2.5 h under supercritical conditions and by gassing out the samples for 55 min.

3.5 Characterization of the Po-net and Al-Po-net porous networks

The synthesized porous Po-net and Al-Po-net networks was characterized in order to determine their permanent porosity and surface area. After solvent removal under supercritical conditions using liquid CO_2, the open pore structure of the Po-net and Al-Po-net networks was obtained. Nitrogen adsorption/desorption measurements were used to determine the surface area of the samples, analyzing the results with the BET method.

The BET method was employed for the analysis of the nitrogen sorption measurements in order to determine the surface area of the samples. In Figure 3.2A the adsorption/desorption isotherms of Po-net and Al-Po-net are presented. The porous Po-net network exhibits a high BET area of 623 m^2gr^{-1} with a total pore volume (V_{total}) of 0.70 cm^3/g while, the Al-Po-net network showed a lower BET surface area of 167m^2gr^{-1}.
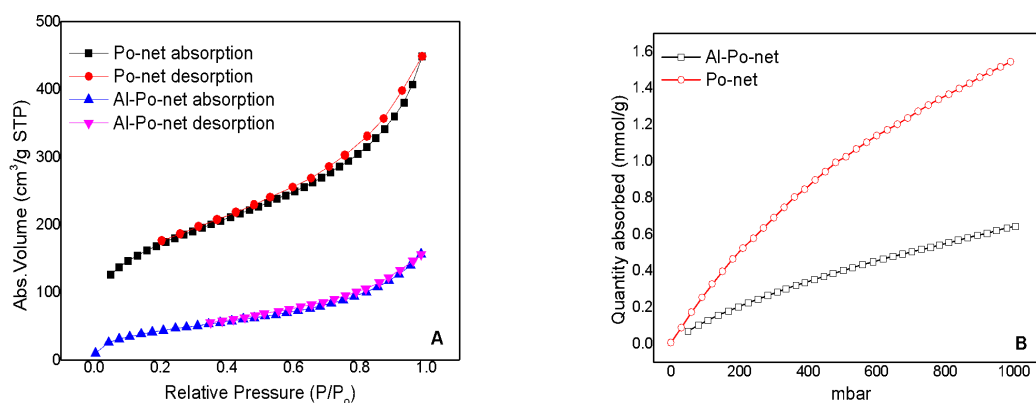

Figure 3.2 (A) Nitrogen adsorption/desorption isotherms at 77 K of the Po-net and Al-Po-net networks and (B) CO_2 adsorption isotherms of the Po-net and Al-Po-net networks at 273 K.

To further examine the ability of the synthesized porous material to capture CO_2, adsorption isotherms were measured at 273 K (Figure 3.2B). The porous Po-net network shows a higher

24

CO_2 adsorption capacity of 1.54 mmol/gr at 990 mbar while, the Al-Po-net network shows a lower CO_2 adsorption capacity of 0.63 mmol/g at the same pressure.

The chemical composition of the Po-net and Al-Po-net networks was characterized by Fourier transform infrared (FTIR) spectroscopy and diffuse reflectance UV/vis spectroscopy (Figure 3.3) The FTIR spectrum of the Po-net network showed a vibration peak at 3313 cm^{-1} attributed to the secondary amine bond, N-H, of the pyrrole ring (Figure 3.3A). The typical vibration peak at 2925 cm^{-1} were assigned to the C-H stretching mode from the pyrrole and benzene rings. The C=N and C=C stretching vibrations of the porphyrin macrocycle and the benzene ring appeared at 1740, 1667, 1499,1469 cm^{-1}.[1] The FTIR spectrum of Po-net was almost identical to that of Al-Po-net except for the peak at 1667 cm^{-1}, assigned to the vibration of the C=N bond of the pyrrole ring indicating the complexation of the aluminum ions by the porphyrin ring of Po-net.
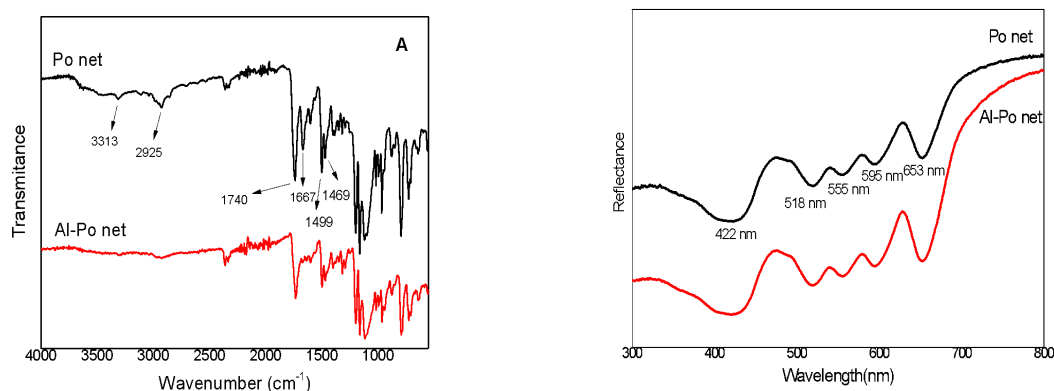
Figure 3.3 (A) FTIR spectra of the Po-net (black line) and Al-Po-net (red line) network and (B) diffuse reflectance UV-Vis spectra of the polymer networks.

Figure 3.3B depicts the diffuse reflectance UV/Vis spectra of the two polymer networks. The UV/Vis absorption spectrum of the porphyrin macrocycle exhibits an intense feature at about 422 nm (the "Soret" band), followed by several weaker absorptions (Q bands) at higher wavelengths (518 nm, 555nm, 595 nm and 653 nm). Similar was the spectrum of the Al-Po-net network signifying that the metal complexation did not alter the absorption behavior of the porphyrin ring.

Furthermore, EDS analysis confirmed the presence of aluminum in the porphyrin network with a 2.48 wt% Al with respect to 97.5 wt% carbon. (Figure 3.4A). The SEM images in Figure 3.4 B and C show the morphology of the Po-net and Al-Po-net networks.

(A)
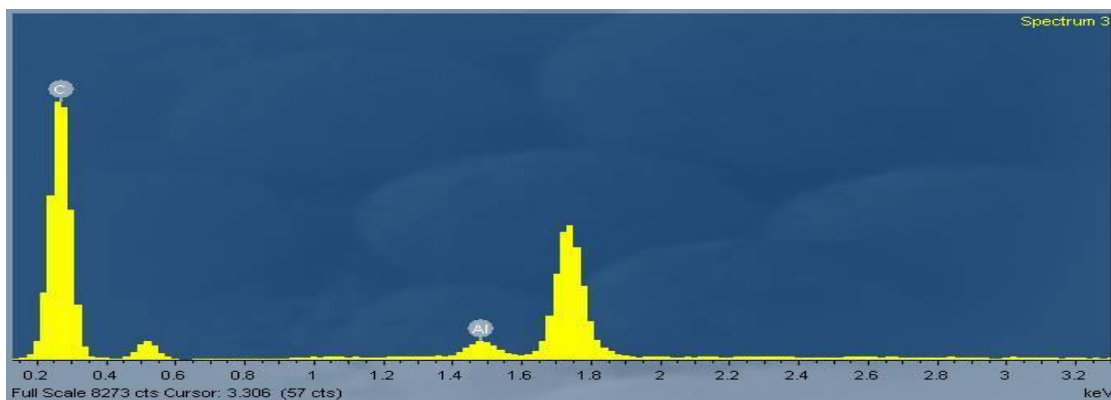
(B)
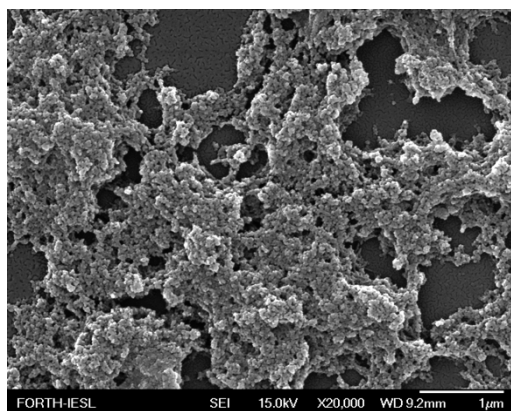
(C)

Figure 3.4 (A) EDS analysis for Al-Po-net, and (B), (C) SEM images of the Po-net and Al-Po-net network, respectively.

3.6 Catalytic performance of the Po-net and Al-Po-net networks

Next the catalytic activity of Po-net and Al-Po-net were examined in the cycloaddition reaction of CO_2 to epichlorohydrin to produce the cyclic carbonate under ambient pressure at different reaction temperatures.
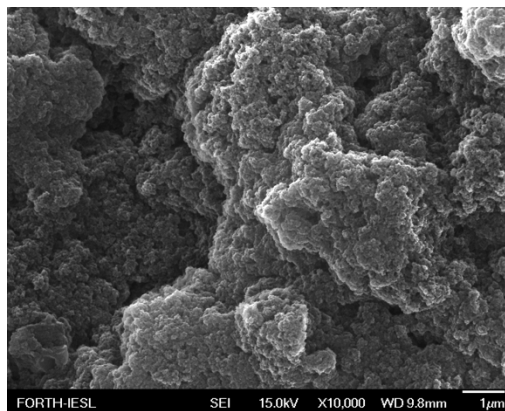
The conversion of the reaction was determined by ^{1}H NMR spectroscopy. The ^{1}H NMR spectra of the reaction mixture show the appearance of new peaks assigned to the protons of the cyclic carbonate, while at the same time the peaks assigned to the protons of epichlorohydrin decrease. Figure 3.8 shows a typical NMR spectrum of a catalytic reaction mixture. The conversion yield was calculated by ratioing the integrals of the peaks 3 to a.
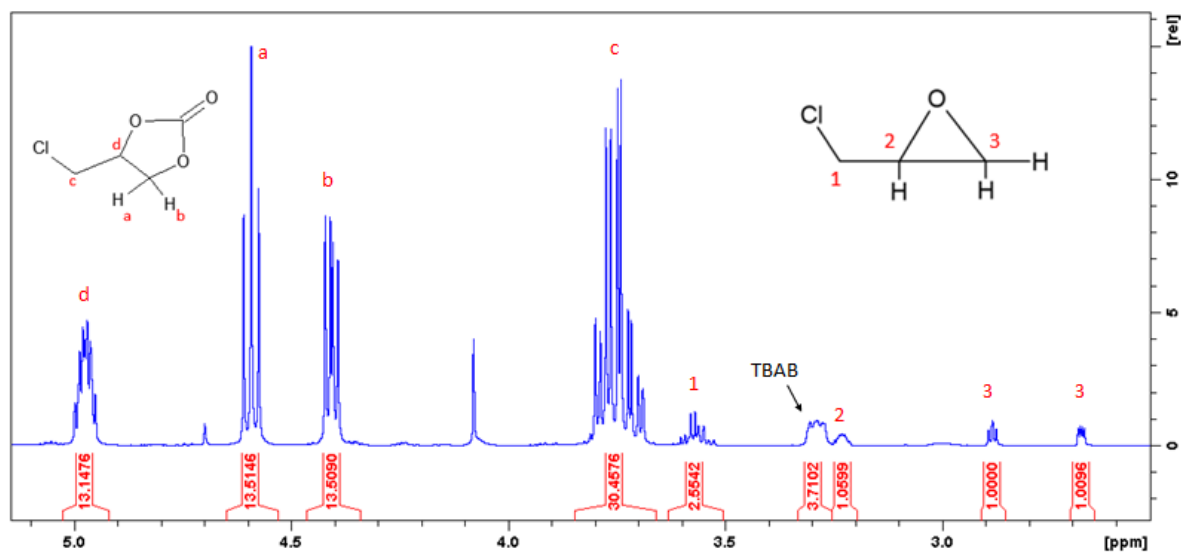

Figure 3.5 A typical ^{1}H NMR spectrum of the reaction mixture using Po-net as the catalyst.

Table 3 shows the reaction yield for three different temperatures (30, 80 and 100 °C) at constant pressure (1 atm). The epichlorohydrin to catalyst molar ratio in all reactions was kept constant at 400 and the molar ratio of epichlorohydrin to the co-catalyst was 50 in all reactions. The

catalytic activity of both Po-net and Al-Po-net was compared to the activity of TBAB alone at the same reaction conditions and to the activity of the catalyst in the absence of TBAB.
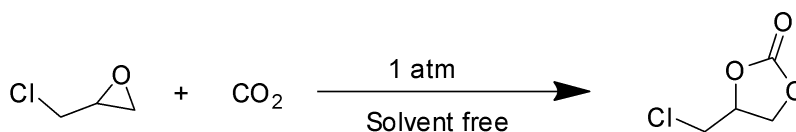
Table 3. Cycloaddition of CO_2 to epichlorohydrin to form cyclic carbonate at different reaction conditions[a]						
Entry	Catalyst	Co-catalyst	Temperature (°C)	Pressure (atm)	Time (h)	Conversion % [b]
1	Po-net	TBAB	30	1	24	31
2	Al-Po-net	TBAB	30	1	24	21
3	-	TBAB	30	1	24	19
4	Po-net	TBAB	80	1	24	65
5	Al-Po-net	TBAB	80	1	24	60
6	-	TBAB	80	1	24	64
7	Po-net	-	80	1	24	31
8	Al-Po-net	-	80	1	24	0
9	Po-net	TBAB	100	1	24	88
10	Al-Po-net	TBAB	100	1	24	93
11	-	TBAB	100	1	24	82
12	Po-net	-	100	1	24	21
13	Al-Po-net	-	100	1	24	1

(a) Reaction conditions: 3.2 mmol epichlorohydrin, catalyst 0.25 mol % with respect to epichlorohydrin, TBAB 2 mol% with respect to epichlorohydrin

(b) Determined by ^{1}H NMR spectroscopy

As seem from Table 3 the conversion increases when increasing the reaction temperature.

In particular, by increasing the temperature from 30 ºC to 100 ºC the conversion increases from 31 % to 88 % and from 21 % to 93 % for the Po-net and the Al-Po-net network, respectively. It is noted that for these temperatures the conversion increases from 19 % to 82 % for TBAB alone.
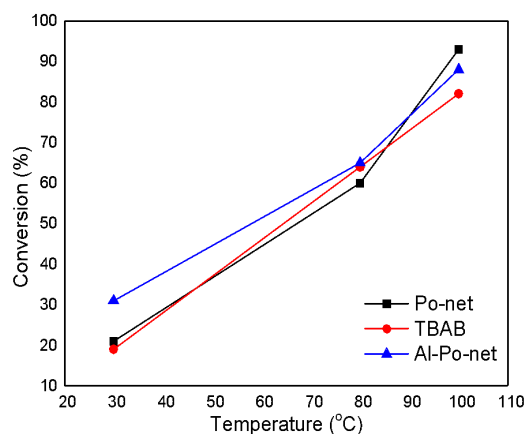

Figure 3.6 Conversion of the cycloaddition reaction of CO_2 to epichlorohydrin catalyzed by TBAB (●), Po-net (■) and Al-Po-net (▲) at different reaction temperature. Reaction conditions: Epichlorohydrin (3.2 mmol), 24 h, 1 atm, catalyst (0.25 mol%), TBAB (2 mol%).

Notably, at 30 ºC both the catalyst as well as the co-catalyst alone exhibit low conversion yields, with the Po-net giving 31 % (entry 1 in Table 3), the Al-Po-net giving 21 % (entry 2 in Table 3) and TBAB in the absence of the catalysts giving 19% (entry 3 in Table 3) conversion. These results show that at low temperature the catalytic reaction is very slow. After this ascertainment a higher temperature (80 ºC) was employed which exhibited higher conversion compared to the reaction at 30 ºC. The conversion of the Po-net network increased to 65 % (entry 4 in Table 3), while the Al-Po-net network and TBAB had 60 % and 64 % conversion, respectively (entries 5 and 6 in Table 3, respectively). Control reactions were also carried out with Po-net and Al-Po-net alone in the absence of TBAB, and with TBAB in the absence of any catalyst, Po-net or

Al-Po-net, and are presented in Table 3 (entries 3, 6-8 and 11-13). These results signify the importance of TBAB in the cycloaddition reaction of CO_2 to epichlorohydrin.

The second parameter investigated in this reaction was the amount of co-catalyst present in the reaction medium. Table 4 shows the reaction conversion for two different amounts of TBAB with respect to epichlorohydrin (1 and 2 mole%) at a reaction temperature of $100\,^\circ C$. The results show a significant increase of the conversion when the moles of TBAB increased from 1 % to 2 % for all reactions.
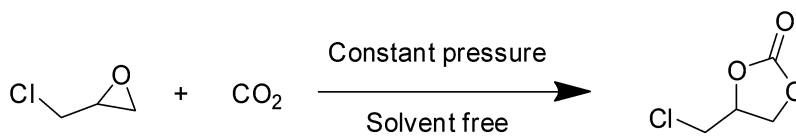
Table 4. Cycloaddition of CO_2 to epichlorohydrin to form the cyclic carbonate at different reaction conditions.[a]						
Entry	Catalyst	Co-catalyst	Temperature (°C)	Pressure (atm)	TBAB Moles %[c]	Conversion % [b]
1	Po-net	TBAB	100	1	1	64
2	Al-Po-net	TBAB	100	1	1	69
3	-	TBAB	100	1	1	55
4	Po-net	TBAB	100	1	2	88
5	Al-Po-net	TBAB	100	1	2	93
6	-	TBAB	100	1	2	82
(a) Reaction conditions: 100 °C, 1 atm, 3.2 mmol epichlorohydrin, catalyst 0.25 mol% (b) Determined by ^1H NMR spectroscopy						

Figure 3.7 Conversion of the cycloaddition reaction of CO_2 to epichlorohydrin catalyzed by TBAB (■), Po-net (●) and Al-Po-net (▲) for different amounts of co-catalyst. Reaction conditions: epichlorohydrin 3.2 mmol, CO_2 1 atm, 24 h, catalyst 0.25 mole%, temperature 100 ºC.

Figure 3.7 shows a very high increase of the conversion of the reaction for all catalysts as the amount of co-catalyst increase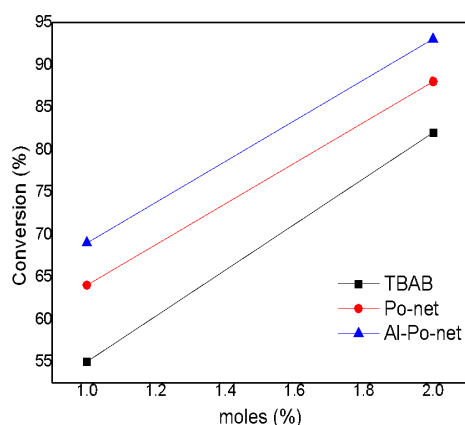d from 1 mole% to 2 mole% with respect to epichlorohydrin. For Po-net the conversion increased from 64 % (entry 1, Table 4) to 88 % (entry 4, Table 4), while for Al-Po-net the conversion increased from 65 % (entry 2, Table 2) to 93 % (entry 5, Table 4). It is noted that for TBAB alone in the absence of any catalyst the conversion increased also from 55% (entry 3, Table 4) to 82 % (entry 6, Table 4).

Finally, to further evaluate the catalytic behavior of the polymer networks, a kinetic study was conducted under 1 atm, at 100 ºC, using 0.25 mole % catalyst and 2 mol% co-catalyst. The results from the kinetic study are presented in Table 5.
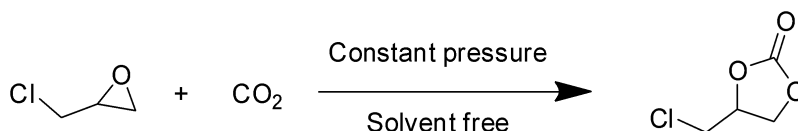

Table 5. Cycloaddition reaction of CO_2 to epichlorohydrin to form the cyclic carbonate. [a]						
Entry	Catalyst	Co-catalyst	Temperature	Pressure	Time	Conversion % [b]

			(ºC)	(atm)	(h)	
1	Po-net	TBAB	100	1	1	61
2	Al-Po-net	TBAB	100	1	1	39
3	-	TBAB	100	1	1	58
4	Po-net	TBAB	100	1	4	73
5	Al-Po-net	TBAB	100	1	4	59
6	-	TBAB	100	1	4	74
7	Po-net	TBAB	100	1	15	87
8	Al-Po-net	TBAB	100	1	15	88
9	-	TBAB	100	1	15	78
10	Po-net	TBAB	100	1	24	88
11	Al-Po-net	TBAB	100	1	24	93
12	-	TBAB	100	1	24	82
13	Po-net	TBAB	100	1	48	93
14	Al-Po-net	TBAB	100	1	48	91
15	-	TBAB	100	1	48	76

(a) Reaction conditions: 100 ºC, 1 atm, 3.2 mmol epichlorohydrin, catalyst 0.25 mol%, TBAB 2 mol%

(b) Determined by ^{1}H NMR spectroscopy

From the above results it is observed that the conversion of epichlorohydrin to the cyclic carbonate proceeds quickly within the first 1 h with the Po-net giving a 61 % (entry 1 in Table 5) conversion, the Al-Po-net a 39 % (entry 2 in Table 5) conversion and TBAB in the absence of any catalyst 58 % (entry 3 in Table 5) conversion, while in 24 h the reaction is complete for both catalysts. Figure 3.8 shows a typical conversion over time curve for the three catalytic reactions.
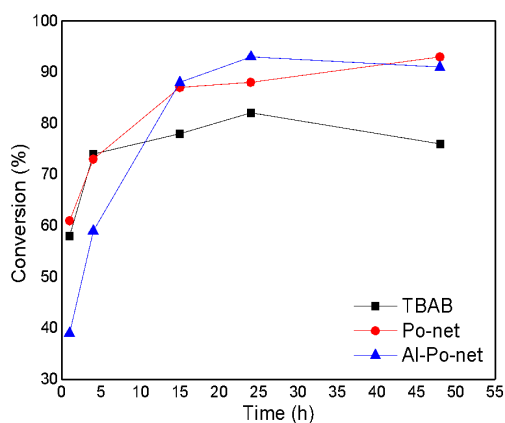
Figure 3.8 Conversion over time for the cycloaddition reaction of CO_2 to epichlorohydrin catalyzed by TBAB (■) , Po-net (●) and Al-Po-net (▲). Reaction conditions: Epichlorohydrin 3,2 mmol, 100 ºC, CO_2 1 atm, catalyst 0.25 mol%, TBAB 2 mol%.

When the reaction was allowed to proceed for 4 h, TBAB alone and the Po-net network showed an increase in conversion to 74 % (entry 6, Table 5) and 73 % (entry 4, Table 5), respectively while, the Al-Po-net shows a lower conversion yield of 59 % (entry 5, Table 5) which indicated that the Al-Po-net catalyst proceeds with lower kinetic rates. Given that information, the catalysts were investigated for longer time. At 15 h it is clear that TBAB has started to reach a plateau with a conversion of 78 % (entry 9, Table 5) while, the conversion of the Po-net catalyst was 87 % (entry 7, Table 5) and for Al-Po-net am increase to 88 % (entry 8, Table 5) conversion was found. Furthermore, the reaction was allowed to proceed for 24 h, and showed a small further increase of the conversion for TBAB at 82 % (entry 12, Table 5), whereas, the Po-net reached a plateau at 88% (entry 10, Table 5) conversion and Al-Po-net gave 93 % (entry 11, Table 5) conversion. Finally, the behavior of the catalysts was investigated at longer time to examine if they have reached the highest conversion. As it is shown in Figure 3.7A when used alone TBAB after 48 h shows a small decrease of the conversion to 76 % (entry 15, Table 5), while Po-net gives a small increase of the conversion to 93 % (entry 13, Table 5) and Al-Po net seems to have reached a plateau at 91 % conversion (entry 14, Table 5). The above results show that the catalytic conversion of epichlorohydrin to cyclic carbonate reached the maximum conversion within 24 h for both the porous porphyrin networks. In general Al-Po-net showed a

better catalytic activity compared to Po-net at 30 ℃, 80 ℃ and 100 ℃ and for both co-catalyst concentrations. However, a higher catalytic activity of Po-net is observed at low reaction times (1 h, 4 h and 15 h) which can be attributed to the higher surface area of the Po-net network.

3.7 References

[1] Behling R, Valange S, Chatel G. Heterogeneous catalytic oxidation for lignin valorization into valuable chemicals: what results? What limitations? What trends? *Green Chem*. 2016;18(7):1839-1854.

[2] Chen Y, Luo R, Xu Q, Zhang W, Zhou X, Ji H. State-of-the-Art Aluminum Porphyrin-based Heterogeneous Catalysts for the Chemical Fixation of CO_2 into Cyclic Carbonates at Ambient Conditions. *ChemCatChem*. 2017;9(5):767-773.

4. Conclusions

This thesis reports the successful synthesis of porphyrin networks and aluminum porphyrin networks that are potential candidates for gas capture and conversion applications. A simple free radical polymerization was employed in order to produce porphyrin networks (Po-net), while the Al-Po network was obtained by the metalation of Po-net with dimethylaluminum chloride. The morphology of the networks was investigated by SEM. Solid open-pore gels were obtained using supercritical point drying with liquid CO_2 to dry the samples from EtOH. The porosity and surface area of the networks were investigated by N_2 adsorption/desorption isotherms, analyzed using the BET method, while their CO_2 adsorption capacity was investigated by CO_2 adsorption measurements.

The Po-net showed a high BET surface area of 622 m^2g^{-1} (after supercritical CO_2 drying), while the Al-Po-net showed a lower BET surface area of 167 m^2g^{-1} after drying under the same conditions. CO_2 adsorption measurements showed that the Po-net exhibits 1.54 mmol/g adsorption at 273 K in comparison with the Al-Po-net which showed an adsorption of 0.63 mmol/g at 273 K. It is thus concluded that the Po-net network exhibits a higher ability to adsorb CO_2 compared to the Al-Po-net network, possibly due to the higher surface area of the former network.Finally, the catalytic performance of both network was evaluated in the cycloaddition reaction of CO_2 to epichlorohydrin using tetrabutylammonium bromide (TBAB) as the co-catalyst. The experimental results showed a high catalytic performance of the Al-Po-net network with a 93% conversion at 100 ºC, 1 atm and 24 h reaction time, while the Po-net exhibited good performance with a 88% conversion at 100ºC, 1 atm and 24 h. These results suggest that the porphyrin-based and aluminum porphyrin-based networks are potentially attractive candidates for carbon dioxide capture and conversion.

Appendices

5. Characterization techniques

5.1 Scanning Electron Microscopy (SEM)

The scanning electron microscope is designed to provide high-resolution, high-magnification images of a sample placed on a surface, even though it operates at low electron beam currents. A tungsten filament emits electrons, which are focused by an electronoptical system. The electron beam can scan the sample surface and can provide composition at a point, along a line or over a rectangular area, by scanning the beam across the surface in a series of parallel lines. The sample is mounted on a stage that can be accurately moved in all three directions (x, y and z), normal to the plane of the sample. SEM can produce magnified images from virtually any type of specimen. The instrument generally operates in a high vacuum and a very dry environment in order to produce the high energy beam of electrons needed for imaging. Thus, most specimens destined for study in the SEM are poor conductors, with a few notable exceptions. In the SEM, the imaging system depends on the specimen being sufficiently electrically conductive to ensure that the bulk of the incoming electrons go to ground. The formation of the image depends on collecting the different signals that are scattered as a consequence of the high electron beam interacting with the sample. The two principal signals used to form images are backscattered electrons and secondary electrons generated within the primary beam-sample interactive volume. The backscattered electron coefficient increases with increasing atomic number of the specimen, whereas the secondary electron coefficient is relatively insensitive to atomic number. This fundamental difference in the two signals has an important effect on the way samples may need to be prepared. The use of scanning electron microscopy may be considered when being able to interpret the information obtained from the SEM and attempt to relate the form and structure of the two-dimensional images and identity, validity and location of the chemical data back to the three-dimensional sample from which the information was derived. A schematic representation of a SEM setup in depicted in Figure 5.1.
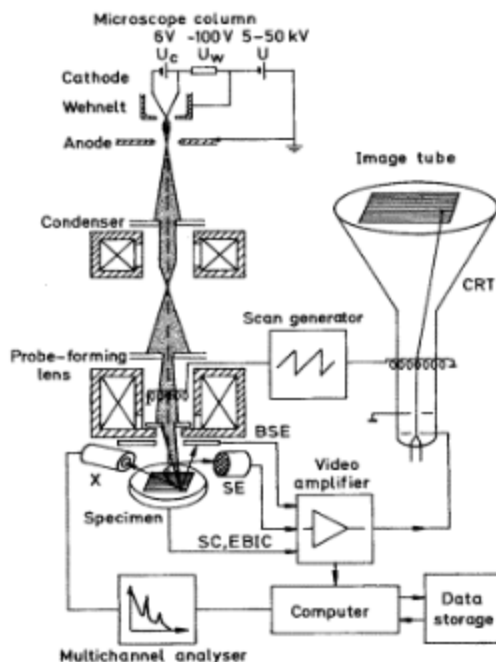
Figure 5.1 Schematic representation of a typical SEM setup

5.2 ^{1}H NMR spectroscopy

NMR spectroscopy is a very useful and common technique for the structural characterization of chemical compounds.[1] ^{1}H NMR and ^{13}C NMR are the more commonly used for the characterization of materials. NMR spectroscopy is based on the principal of nuclei being positively charged spinning on an axis and forming a tiny magnetic field. This nuclear magnetic field can either align or oppose with an external magnetic field Bo (Figure 5.2).

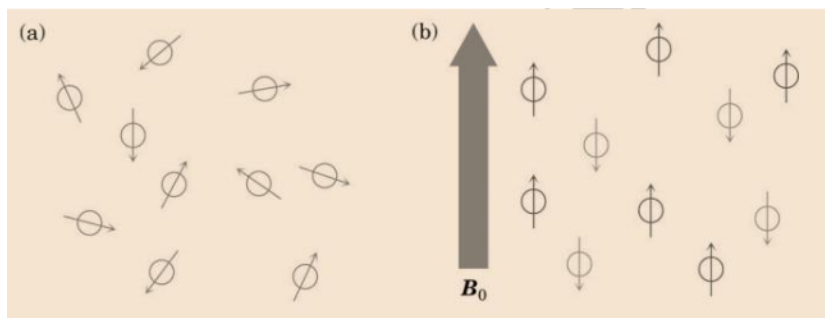

Figure 5.2 (a)Random orientation of the nuclear magnetic fields in the absence of an external magnetic field (Bo), (b) Aligned or opposed nuclear magnet fields in the presence of an external magnetic field (Bo).

Different nuclei absorb electromagnetic irradiation at different wavelength depending on the chemical and electronic environment. The position and the pattern of the NMR signal provide the required information regarding the environment of the nuclei. The exact field strength (in ppm) of a nucleus comes into resonance relative to a reference standard, usually the signal of the deuterated solvent used. Electron clouds "shield" the nuclei from the external magnetic field causing them to absorb at higher energy (lower ppm) whereas the neighboring functional groups "deshield" the nuclei causing them to absorb at lower energy (higher ppm). Chemically and magnetically equivalent nuclei resonate at the same energy and give a single signal or pattern. Protons on adjacent carbons interact and "split" each other's resonances into multiple peaks following the n + 1 rule with a coupling constant J. Spin-spin coupling is commonly observed between nuclei that are one, two and three bonds apart. The area under an NMR resonance is proportional to the number of nuclei that give rise to that resonance, thus by integration the protons of that resonance can be calculated.

5.3 Attenuated Total Reflectance (ATR)-FTIR spectroscopy

ATR-FTIR spectroscopy is a sampling technique used in conjunction with infrared spectroscopy. It is widely used to examine a variety of samples such as solids, powders, pastes and liquids without further preparation. An attenuated total reflection accessory operates by measuring the changes that occur in a totally internal reflected infrared beam when it comes in contact with a sample which is placed on a high refractive index crystal. Typical materials for ATR crystals include germanium, zinc selenide or diamond. The later has excellent mechanical properties which make it an ideal material for ATR. In the case of a liquid sample, pouring a very small amount over the surface of the crystal is sufficient. If the sample is solid, it is pressed into direct contact with the crystal.

An infrared beam is directed onto a high refractive index crystal at a certain angle. Due to the nature of the ATRP crystal, the refractive index of the analyzed sample will have a lower refractive index than the refractive index of the crystal. Under these conditions total internal reflection can occur at a certain angle of incidence at the interface between the two media. This

internal reflectance creates an evanescent wave that extends only a few microns beyond the surface of the crystal into the sample. In the regions of the infrared spectrum where the sample absorbs energy, the evanescent wave will be attenuated. The beam is then collected by a detector as it exits the crystal and the infrared spectrum of the samples is generated.

5.4 Types of adsorption isotherms

Two types of adsorption isotherms have been identified; physical and chemical isotherms. Adsorption isotherms, mainly resulting from physisorption, have a variety of forms and the majority of them can be grouped into one of the six types classified by IUPAC. The first five types (I to V) are referred as the Brunauer classification. The IUPAC classification (1985) introduced a more recent type of physisorption isotherm (type VI) (Figure1.2a).[2]
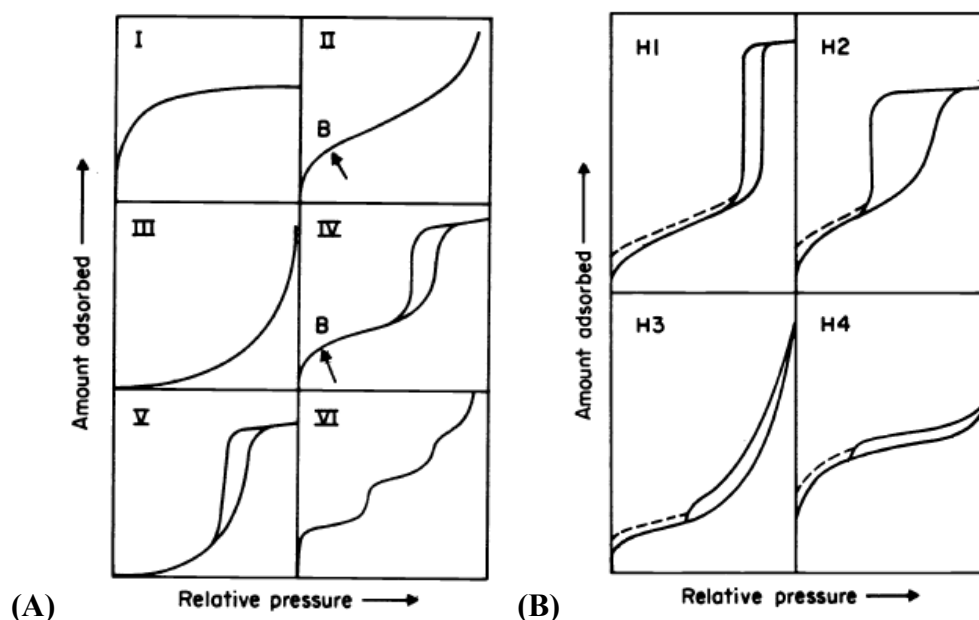

Figure 1.2 (A) main types of adsorption isotherms and (B) the four types of hysteresis loops based   on the IUPAC classification.

Type I isotherm is concave to the relative pressure (p/p0) axis. The isotherm curve rises sharply at low relative pressure range until it reaches a plateau when the p/p0 goes to 1. The narrow range of relative pressure required to obtain this plateau is an indication of a limited range of

pore size. Plus the horizontal appearance of the plateau depicts a small external surface area. As a result the limiting adsorption is dependent on the available micro-pore volume.

Type II isotherm is at the beginning concave to the relative pressure (p/p0) axis, then becomes linear and at high pressure close to 1 is convex to the (p/p0) axis. This formation indicates the presence of an adsorbed layer with progressively increasing thickness. If the knee of the isotherm is sharp, the uptake at point B (the beginning of the linear section) is considered to represent the completion of the monolayer and the beginning of the multilayer. These types of isotherms are obtained for non-porous or macro-porous adsorbents that allow unrestricted monolayer-multilayer adsorption and complete reversibility of the adsorption-desorption isotherm (absence of hysteresis).

Type III isotherm is convex to the relative pressure (p/p0) axis over the complete range, therefore has no point B. These isotherms are not common since they are assigned to weak adsorbent-adsorbate interactions.

Type IV isotherm is at the initial region very similar to the type II but tends to level off at a small plateau at high relative pressures. It exhibits a hysteresis loop that is usually associated with the filling and emptying of the mesopores by capillary condensation. The lowerbranch represents measurements obtained by progressive addition of gas of the adsorbent whereas the upper branch by progressive withdrawal. Type IV isotherms are very common but the hysteresis loops vary according to each system and can be categorized in four types (Figure 1.2b).

Type V isotherm is convex to the relative pressure (p/p0) axis at the first part and levels off at high relative pressure. As type III these isotherms are very rare. This isotherm type is associated with weak adsorbent-adsorbate interactions and the hysteresis loop is formed according to pore filling and emptying mechanisms.

Type VI isotherm is also relatively rare and it is also known as stepped isotherm. It is associated with layer-by-layer adsorption on a highly uniform surface. The sharpness of the steps is dependent on the system and the temperature.

Hysteresis loops are associated with capillary condensation and they usually are distinctive and reproducible for meso-porous systems. There are many different forms of loops reported in the literature but are all mainly classified into four major categories according to the IUPAC classification. Type H1is a narrow loop with perpendicular and nearly parallel adsorption-desorption branches. This type of loop is obtained from systems with a narrow distribution of uniform pores. Type H2 loop is very broad with a long nearly flat plateau and a steep desorption branch. H2 loops are obtained from materials with a complex pore structure that exhibit interconnected pore networks of different size and shape. Type H3 and H4 loops are very similar since both do not terminate in a plateau at high relative pressure. They are usually obtained by aggregates of particles or adsorbents containing slit-shaped pores but in H4 loops the pore size distribution is mainly attributed to micro-pores.

5.5 References

[1] Mcmurry J., Organic Chemistry, 2012.

[2] Lykiema J, Sing KSW, Haber J, et al. Prepared for publication by the Subcommittee on Reporting Gas Adsorption Data Consisting of K. S. W. SING (UK, Chairman); D. H. Everett (UK); R. A. W. Haul (FRG); L. Moscou (Netherlands); R. A. Pierotti (USA); J. Rouquerol (France); T. Siemieniewska (Poland), 1984:17.